Interfacial Curvature in Graft and Diblock Copolymers and Implications for Long-Range Order in Cylindrical Morphologies

Samuel P. Gido*

Department of Polymer Science and Engineering, W. M. Keck Electron Microscopy Laboratory, University of Massachusetts Amherst, Amherst, Massachusetts 01003

Zhen-Gang Wang

Division of Chemistry and Chemical Engineering, California Institute of Technology, Pasadena, California 91125

Received March 14, 1997; Revised Manuscript Received September 2, 1997[⊗]

ABSTRACT: Microstructures of block copolymers in the strong segregation limit are characterized by well-defined interfaces separating the different block materials into domains on a nanometer scale. In this paper, we address the effects of architectural and conformational asymmetry of the blocks on the interfacial curvature characteristics and on the degree of long-range order in the cylindrical morphologies. Experimental (TEM and SAXS) curvature data from polyisoprene−polystyrene (I_2S) simple graft block copolymers and from polyisoprene−poly(*tert*-butyl methacrylate) (PtBMA) linear, conformationally asymmetric diblock copolymers are presented and compared to data from polyisoprene−polystyrene linear diblock copolymers. The experimental data are elucidated by a simple curvature free energy model which accounts for core-space-filling without explicitly specifying the shape of the microdomain. This model allows the prediction of preferred interfacial curvature characteristics as a function of molecular architecture. Good agreement is obtained between the theoretically calculated mean and Gaussian curvatures and the experimentally measured values. A key finding is that the degree of frustration, as measured by the difference between the free energy of the preferred curvature of a given block copolymer and that of the nearest accessible space-filling structure (such as the cylindrical structure), is correlated with the degree of long-range order.

Introduction

In the strong segregation regime of block copolymers, the different monomer domains are separated by well-defined intermaterial dividing surfaces. These internal interfaces can be described by their mean and Gaussian curvatures, which constitute an integral part in the characterization and understanding of the morphologies formed by block copolymers. In this paper, we report results of measured curvature data for graft polyisoprene−polystyrene I_2S block copolymers and for conformationally asymmetric polyisoprene−poly(*tert*-butyl methacrylate) (PtBMA) diblock copolymers. The interfacial curvature is measured through morphological investigation using transmission electron microscopy (TEM) and small angle X-ray scattering (SAXS). Through the variation of conformational asymmetry as well as graft chain architecture we obtain different dependencies of interfacial curvature on block component volume fractions. This interfacial curvature dependence on volume fraction and architecture is manifested in the dependence of observed morphology upon these variables. A mean field model, in the spirit of Semenov,[1] is also formulated, which predicts the preferred mean and Gaussian curvature of the interdomain dividing surfaces, as a function of block copolymer molecular characteristics. The results of these calculations agree very well with the experimentally measured interfacial curvatures.

In our previous experimental study of architecturally asymmetric, graft copolymers, we noticed a large difference in the degree of long-range order of cylindrical morphologies depending on which component was in the corona and which was in the core of the domains.[2] The graft architecture of these I_2S polyisoprene (I)−polystyrene (S) block copolymers is illustrated in Figure 1. When the two PI blocks are on the outside of the cylinders, the structures formed have remarkable long-range order even without special sample preparation techniques such as melt shearing or roll casting.[3,4] When the single PS block is on the outside of the cylinders, long-range order is poor or even nonexistent, in the case of the randomly oriented wormlike micelle structure observed in one of our samples.[5] Similar effects of architecture on long-range order were observed by Hadjichristidis, Lohse, *et al.* in their investigations of the morphologies formed by I_3S miktoarm star block copolymers.[6] Additionally, we have observed an effect of conformational asymmetry in linear diblock copolymers on the degree of long-range order of cylindrical micelles.[7] When the stiffer chain is in the cylinder corona, the samples form lattices with tremendous long-range order even without shearing. When the more flexible chain is in the corona the long-range order is much poorer. In this paper we will see how ideas of preferred interfacial curvature can shed light on the effects of molecular architecture on the ability to form long-range order. We will show that the difference between the free energy of the preferred curvature of a given block copolymer and that of the nearest accessible space-filling structure is correlated with the degree of long-range order. Other influences on long-range order include thermally activated lattice vibrations (phonons) during annealing, which combine with curvature frustration to influence the degree of long-range order which the sample may obtain. These phonon-like fluctuations are determined by the elastic moduli associated with the various modes of lattice distortion, the calculation of which is beyond the scope of this paper. However, it is possible that the curvature frustration could be manifested in the elastic moduli, so that the phonon-type deformations could also be partially rooted in the curvature frustration. Grain structure, formed by the

* To whom correspondence should be addressed.

[⊗] Abstract published in *Advance ACS Abstracts,* October 15, 1997.

S0024-9297(97)00356-2 CCC: $14.00

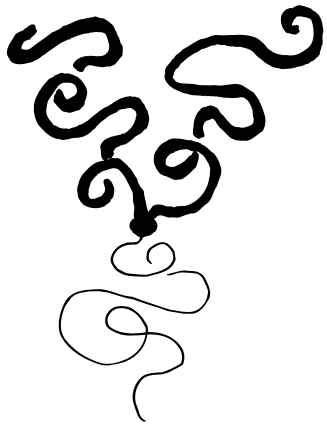

Figure 1. I_2S graft block copolymer architecture. The dark lines represent PI blocks and the light line represents the PS graft block.

kinetics of microphase separation, is also superimposed upon the interfacial curvature and phonon-driven aspects of the structural evolution to produce the final, often complex, morphology. Grain structure and the defects associated with it produce disorder that is generally on a much larger length scale than that effected by the local domain packing considerations on which this study is focused.

The mean and Gaussian curvatures calculated from the model represent the preferences of a single block copolymer chain in a microphase-separated structure. This curvature preference will be seen to be a function of all aspects of block copolymer architecture, including volume fractions, chain stiffnesses, and monomer volumes of the block materials, as well as variations in the connectivity of the blocks such as graft or star block copolymer structures. The curvature preferences define a preferred Gaussian wedge shape for the block copolymer, which is analogous to the shape parameter commonly used for surfactants in micelles and microemulsions.[8,9] The individual chain curvature preference, or wedge shape preference, does not reflect the additional structural constraints necessary in order for the block copolymer material to fill space to constant density and form a lattice structure with long-range order. The preferred wedge shape represents a state of minimized chain conformational and interfacial free energy for a single chain in microphase-separated domains. Packing chains on a lattice will generally lead to slightly different wedge shapes, which also may vary depending on their location in the structure. Experimentally we find, however, that there is a strong correlation between the interfacial mean curvature found in microstructured diblock and graft block copolymer morphologies with long-range order and the preferred interfacial curvature. Presumably, the microphase-separating block copolymer selects, from the available space-filling structures, that structure which minimizes the sum of distortions of all the chains in the system from the preferred wedge shape. This is equivalent to selecting the structure that minimizes free energy.

It has been experimentally observed that microphase-separated diblock copolymers in the strong segregation limit tend to have their microdomains bounded by interfacial surfaces of constant mean curvature.[10−13] The mean curvature, usually denoted by the symbol H, is defined at every point on a surface as the arithmetic mean of the two principal curvatures that are the reciprocals of the two principal radii of curvature.[19] Spheres, cylinders, and the flat plane interfaces of the lamellar morphology are particularly simple examples of constant mean curvature surfaces in which it is intuitively obvious that the locally defined curvature is not varying from place to place on the surface.

Long before their discovery in materials interfaces, constant mean curvature surfaces were known to mathematicians as solutions to a family of variational problems involving minimization of interfacial area required to partition regions of space of specified relative volumes.[20,21] The analogy between a block copolymer with fixed volume fractions trying to reduce its interfacial energy/area and this mathematical problem has been used to formulate a qualitative explanation for the constant mean curvature interfacial geometries observed.[13] However, this analogy is imperfect since in block copolymers interfacial area per chain is coupled to chain stretching through a conservation of volume constraint. There is no analog of chain stretching in the mathematical problem leading to constant mean curvature surfaces. The introduction of chain stretching into the problem can have two different effects. First, the covalent bond between the blocks, and the resulting chain stretching, limit the length scale of microphase separation in block copolymers. The second effect chain stretching can have on microphase-separated morphologies is to cause deviations of interfacial surface geometry from constant mean curvature (CMC). However, the presence of chain stretching does not, by itself, cause a deviation from CMC geometry. It is the interaction of the space-filling packing constraints on a hexagonal, or cubic, lattice with the chain stretching that results in deviations from CMC. This effect has been shown experimentally for triblock materials[22] and, more recently, theoretically for diblocks.[23] Matsen and Bates have recently shown that the packing constraints necessary to fill the center of tripod and tetrapod branch point domains can also lead to deviations from CMC. In the lamellar structure, however, the geometry of the one-dimensional lattice does not create any chain-stretching asymmetry in the structure and thus the intermaterial dividing surfaces (IMDS) remain minimal. Also, except in very special cases,[22] the deviations from CMC in typical cylindrical and cubic structures are too small to be observed experimentally given the finite interfacial width and the resolution limitations of the observation techniques (TEM and SAXS). In the present work we are not overly concerned with whether or not interfacial mean curvature is actually constant. Our goal is to compare the calculated curvature preference of the block copolymer with the interfacial curvatures, measured to the resolution possible with SAXS and TEM, in the morphologies actually formed and to understand long-range order formation in terms of preferred curvature.

Experimental Section

Interfacial H and K values were obtained by TEM and SAXS analysis of two series of model block copolymers. The first series consists of nine linear polyisoprene-*b*-poly(*tert*-butyl methacrylate) diblock copolymers which have $\epsilon = (l_1/l_2)^{1/2} = 0.75$, where $l_i = V_i/R_{gi}^2$. Here V_i is the volume of an arm of material i and R_{gi}^2 is the mean-squared radius of gyration of an arm of material i. There is a substantial difference in the Kuhn lengths of these two block materials, 6.9 Å for PI vs 10.6 Å for PtBMA; however, in the computation of ϵ this chain stiffness difference is partially offset by the monomer densities: 4.32 monomers/nm^3 for PtBMA vs 8.04 monomers/nm^3 for PI.[7] The second series consisted of seven symmetric graft block copolymers composed of PI and polystyrene (PS). As illustrated in Figure 1, a PS block is grafted midway along a PI backbone in these materials. Thus, in the notation of

Table 1. I_2S Molecular Characteristics and Interfacial Curvature

sample	vol % d-PS	M_n PS arm	M_n PI arm	M_n total	M_w/M_n	morphology	primary d spacing (Å)	HR_g
I_2S-1	89	87 300	4 600	97 100	1.04	hex cyl	310 ± 5	0.67
I_2S-2	81	79 100	9 600	89 400	1.04	worm cyl		0.40
I_2S-3	62	61 200	14 800	83 000	1.04	lamella	390 ± 5	0
I_2S-4	44	44 400	21 300	82 500	1.04	hex cyl	429 ± 5	−0.20
I_2S-5	31	31 600	26 500	82 600	1.04	hex cyl	380 ± 5	−0.26
I_2S-5	17	21 100	34 700	92 300	1.04	bcc spheres	289 ± 5	−0.73
I_2S-7	8	9 400	39 100	84 300	1.06	bcc spheres	235 ± 5	−1.24

Table 2. PI-PtBMA Molecular Characteristics and Interfacial Curvature

sample	vol % PtBMA	M_n total	M_w/M_n	morphology	primary d spacing (Å)	HR_g
PtBMA-17	17	58 200	1.08	spheres	331 ± 5	−0.90
PtBMA-22	22	53 500	1.18	spheres	349 ± 5	−0.75
PtBMA-27	27	57 700	1.11	spheres	359 ± 5	−0.71
PtBMA-32	32	64 300	1.07	hex cylinders	419 ± 5	−0.30
PtBMA-50	50	61 300	1.23	lamella	393 ± 5	0
PtBMA-60	60	61 800	1.11	lamella	398 ± 5	0
PtBMA-70	70	58 400	1.10	hex cylinders	331 ± 5	0.38
PtBMA-75	75	55 400	1.13	hex cylinders	308 ± 5	0.44
PtBMA-85	85	61 800	1.08	bcc spheres	233 ± 5	0.81

Olvera de la Cruz and Sanchez,[24] these samples are simple graft block copolymers with $\tau = 0.5$. Alternatively one can think of these materials as three-arm miktoarm stars with two equal length arms of PI and one arm of PS. For these systems the conformational asymmetry, as defined by Milner,[25] takes into account the asymmetry in architecture (arm number) as well as chain statistics. For our I_2S materials $\epsilon = (n_1/n_2)(l_1/l_2)^{1/2} = 1.78$, where n_i is the number of arm/blocks of material i. The compositions and molecular weights of both model block copolymer series are listed in Tables 1 (I_2S) and 2 (PI−PtBMA); more detailed molecular characterization data is given in previous publications.[2,7]

The details of sample preparation and morphological characterization are given in previous publications.[2,7] Samples were slowly cast over 7−10 days from 5 vol. % solutions in toluene, which is approximately a nonpreferential solvent for both systems. After casting, sample films 1−3 mm thick were annealed for 1 week in a vacuum oven at about 20 °C above T_g of the more glassy block in each series. This resulted in annealing temperatures of about 120 °C for both sets of samples. After annealing, samples for TEM were cut into 500−1000 Å thick sections using a cryoultramicrotome with a diamond knife, at temperatures of about −100 °C. Samples were stained with OsO_4, which oxidizes the double bonds of the PI blocks in both series of samples and renders them dark relative to the other blocks in TEM micrographs. TEM observation was carried out in a JEOL 100CX operating at 100 kV. SAXS experiments were performed at the University of Massachusetts using a Regaku-Denki low-angle camera with pinhole collimation and a sealed tube Cu Kα X-ray source. Additional SAXS data were collected at the synchrotron radiation source at the Daresbury Laboratory, Warrington, U.K.[2,7]

Experimental Results

Based on our identification of the morphology of each sample using a combination of TEM and SAXS, as well as accurate lattice parameter measurements derived from the SAXS data, and volume fractions determined by careful molecular characterization[2,7] we were able to calculate the curvature characteristics, H and K, for each sample. For spherical domains packed on a bcc lattice (I_2S-6 and -7, and PI−PtBMA-85), the first Bragg peak measured in SAXS is the 110 reflection. The cubic lattice parameter a is calculated as $a = d_{110}\sqrt{2}$, and the radius of the spherical interface is given by $R_s = (3\phi_s/8\pi)^{1/3}a$, where ϕ_s is the volume fraction of the minor component block forming the core of the spheres. Several PI−PtBMA samples (PI−PtBMA-17, -22, and 27) microphase separated to form spherical domains but did not order on a lattice. The single scattering maximum observed in SAXS for each of these samples corresponds to the average distance between sphere centers, a. The radius of the spherical interface in these samples is approximated by $R_s = \phi_s^{1/3}a/2$; H and K for spheres are then given by $(1/R_s)$ and $(1/R_s)^2$, respectively. For cylindrical domains packed on a hexagonal lattice (I_2S-1, -4, and -5, and PI−PtBMA-32, -70, and -75), the first Bragg peak measured in SAXS is the 100 reflection. The hexagonal lattice parameter a is calculated as $a = 2d_{100}\sqrt{3}$, and the radius of the cylindrical interface is given by $R_c = (2\phi_c/\pi\sqrt{3})^{1/2}a$, where ϕ_c is the volume fraction of the minor component block forming the cores of the cylinders. H and K for cylinders are then given by $(1/2R_s)$ and 0, respectively. One simple graft sample, I_2S-2, formed a randomly oriented wormlike micelle structure.[2,5] The radius of curvature of these structures, and thus the interfacial curvature characteristics, were estimated by measurements from TEM micrographs since the SAXS data from these samples did not allow the determination of these parameters.

Tables 1 and 2 give the morphologies, lattice dimensions, and mean curvatures for each sample from our two series of samples. In order to compare the interfacial curvature of our samples with the behavior of more conformationally and architecturally symmetric diblocks, we obtained a survey of compositions, and lattice dimensions from the literature for PS−PI and PS−PB (polybutadiene) diblocks covering a range of molecular weights and morphologies. Interfacial H and K values were calculated from this data; the literature data and the curvatures calculated from it are tabulated in Table 3. Figure 2 is a plot of HR_o, the dimensionless product of mean curvature and root mean square (rms) end-to-end distance (of the unmicrophase-separated block copolymer), vs polystyrene volume fraction for the PS−PI and PS−PB linear diblock data in Table 3. The product HR_o expresses the interfacial mean curvature in terms of a natural length scale of the polymer chains experiencing this curvature. The band of data with $HR_o = 0$ correspond to samples displaying the lamellar morphology. The negative values of HR_o for small PS volume fractions and the positive values for large PS volume fractions are due to the sign convention for interfacial curvature. If we arbitrarily chose to view the interface from one of the two types of microdomains, PS microdomains in this case, then if this microdomain material is on the concave side of the interface, H is considered negative. If the reference microdomain material is on the convex side of the interface, then H is considered positive. Clearly, switching the choice of the reference microphase switches the sign of H. The data in Figure 2 have an approximate inversion center symmetry about the point (0.5, 0). The data plotted in Figure 2 are consistent in trend and actual numerical values with the plot of calculated HR_o for various morphologies given by Matsen and Bates as Figure 1 in ref 23.

Dimensionless Gaussian curvature, KR_o^2, also changes with PS volume fraction for the PS−PI and PS−PB diblocks, reflecting changes in the equilibrium morphology. KR_o^2 is zero

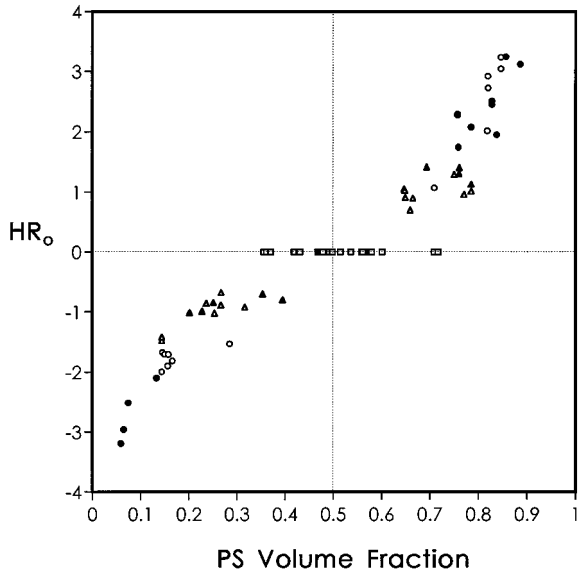

Figure 2. Plot of HR_o vs polyisoprene volume fraction for linear PS−PI and PS−PB diblock copolymers. The data were obtained from the literature and are tabulated in Table 3. Square symbols represent lamellar structures; triangular symbols represent cylindrical structures, and circular symbols represent spherical structures. Open symbols correspond to materials with $N < 1500$, and filled symbols correspond to materials with $N > 1500$.

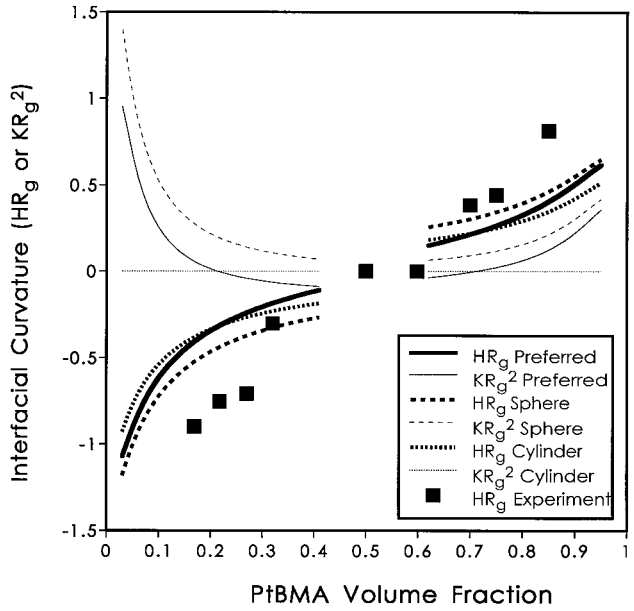

Figure 3. Plots of HR_g and KR_g^2 vs PtBMA volume fraction for PI−PtBMA linear diblock copolymers. The square symbols represent experimentally determined HR_g values. The various lines represent calculated, preferred HR_g and KR_g^2, and cylindrically and spherically constrained HR_g and KR_g^2 values, as indicated by the legend.

in the lamellar region of the morphology diagram around 50/50 volume fractions, it is negative in the bicontinuous region of the morphology diagram, zero again for the cylindrical morphology, and positive for the spherical morphology. The positive KR_o^2 values of the spherical structure become larger as the volume fraction of the minor component decreases toward zero. The sign of K is the same regardless of which microdomain is chosen as the reference.

Figure 3 shows a plot of HR_g vs PtBMA volume fraction for the conformationally asymmetric, linear PI−PtBMA diblock copolymers. Here and throughout the rest of this paper we use R_g rather than R_o as a length scale to nondimensionalize curvatures. Thus in order to compare actual curvature values to Figure 2, one must multiply the HR_g values in Figure 3 by

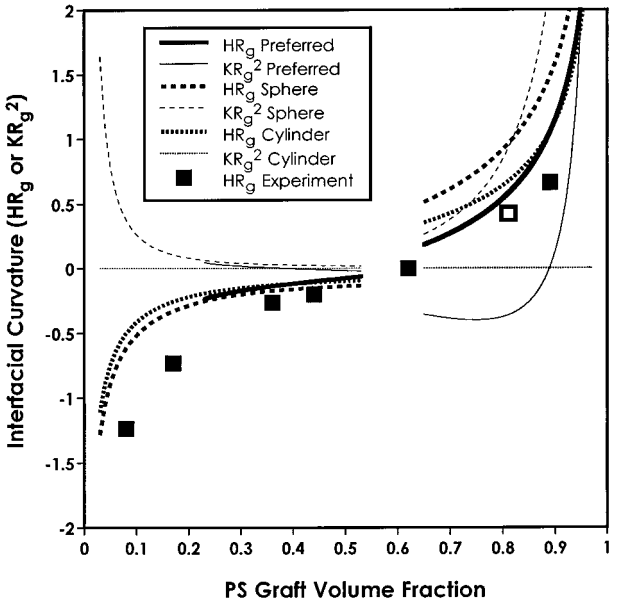

Figure 4. Plots of HR_g and KR_g^2 vs PS graft volume fraction for I_2S graft block copolymers. The filled square symbols represent experimentally determined HR_g values from SAXS data. The unfilled symbol represents the disordered wormlike cylinder structure for which HR_g was determined by measurements from TEM micrographs. The various lines represent calculated, preferred HR_g and KR_g^2, and cylindrically and spherically constrained HR_g and KR_g^2 values, as indicated by the legend.

$\sqrt{6}$. The data follow a similar trend to that observed with PS−PI and PS−PB diblocks. However, in this case the data are less symmetric about 50/50 volume fraction. The curve is shifted slightly so that the negative curvature, using the less flexible PtBMA block as the reference material, persists to higher volume fraction than in the PS−PI and PS−PB cases. At each volume fraction the curvature viewed from the PtBMA microphases is either more negative or less positive than in Figure 2. This effect is due to the greater conformational asymmetry of the PI−PtBMA diblocks.

Figure 4 is a plot of HR_g vs PS graft volume fraction for the I_2S symmetric simple graft block copolymers. Here again we use the unperturbed radius of gyration of the molecules rather than the end-to-end distance as the basis for nondimensionalizing the curvature because of ambiguity about what R_o means for a star-shaped molecule. R_g values for the star-shaped I_2S molecules were calculated using the relationship derived by Zimm and Stockmeyer.[26] In this case, the asymmetry of the data around 50/50 volume fraction is quite pronounced. The curve is shifted so that the negative curvature, using the single PS graft block as the reference material, persists to higher volume fraction than in the PS−PI and PS−PB cases. The data do not pass through zero H until the PS volume faction is about 2/3. At each volume fraction, the curvature, viewed from PS microphases, is either more negative or less positive than in both Figures 2 and 3. This effect is due to the strong asymmetry inherent in the simple graft molecular architecture.

Figure 5 shows TEM micrographs illustrating the pronounced difference in the degree of long-range order between PI−PtBMA diblocks with (a) PI core cylinders (high long-range order), and (b) with PtBMA core cylinders (poor long-range order). The hexagonal geometry evident in the two-dimensional SAXS pattern, inset in Figure 5a, shows the exceptional long-range order displayed by sample PtBMA-70 over volumes of material on the order of a cubic millimeter. Figure 6 shows TEM micrographs illustrating the same effect in I_2S graft materials. Figure 6a shows a projection parallel to the cylinder axis of the extremely well ordered morphology formed by sample I_2S-4, which has a PS volume fraction of 0.44. In this structure, the PS blocks form the cylinder cores and the two PI blocks per molecule are in the corona. The inset two-

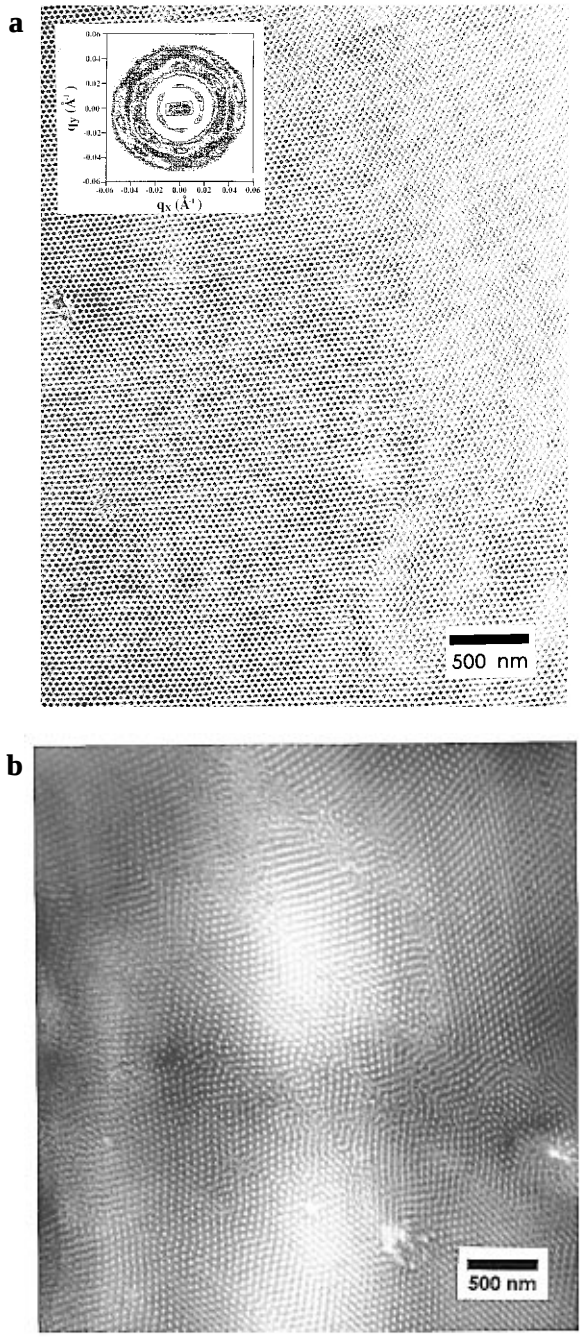

Figure 5. TEM micrographs of PI−PtBMA cylindrical samples: (a) PI−PtBMA-70 cylinders with PI in the core displaying tremendous long-range order. A two-dimensional SAXS pattern of this material is inset. (b) PI−PtBMA-32 cylinders with PtBMA in the core displaying poor long-range order.

dimensional SAXS pattern illustrates that coherent, hexagonal long-range order persists over a macroscopic volume of material. Figure 6b shows the much less ordered cylindrical morphology formed by I_2S-1, which has a PS volume fraction of 0.89. In this sample the two PI blocks per molecule are in the cylinder cores and the single PS block per molecule is in the corona. Figure 6c shows the randomly oriented wormlike cylinder structure formed by I_2S-2. This sample, which displays no long-range order at all, has been analyzed in detail in a separate publication.[5] In the randomly oriented cylinder structure, the two PI blocks are also in the cylinder cores and the single PS blocks are in the coronas.

Interfacial Curvature Modeling

In this section, we calculate the preferred H and K for a given block copolymer material as a function of

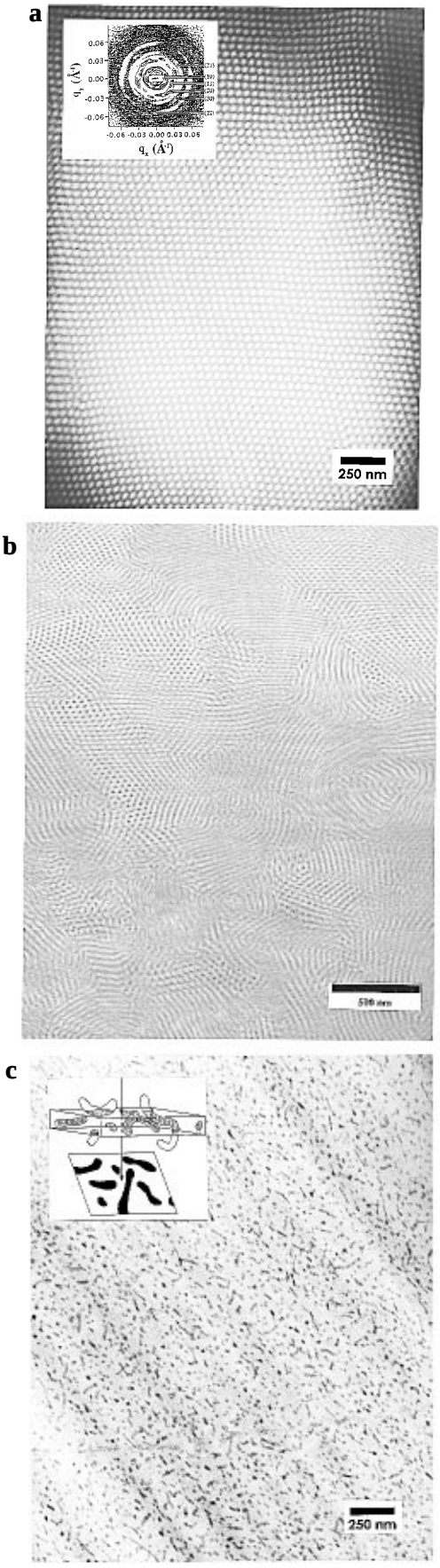

Figure 6. TEM micrographs of I_2S graft block copolymer cylindrical samples: (a) end-on projection of extremely well ordered cylinders of I_2S-4 with PI blocks in the corona (inset: two-dimensional SAXS pattern); (b) poorly ordered I_2S-1 cylinders with PI blocks in the cylinder cores; (c) PI core cylinders formed by I_2S-2 that display a disordered wormlike structure.

volume fractions, block material characteristics, and molecular architecture. This is achieved by formulating a curvature dependent free energy per block copolymer chain in a structure of arbitrary interfacial curvature. This energy is minimized to find the preferred H and K subject to appropriate curvature dependent volume constraints. Two types of constraints will be considered. In the first type of constraint, we specify the three perfect domain shapes—lamella, cylinders, and spheres—and calculate the curvature characteristics and free energies of these specified geometries. The interfacial curvature for the lamellar structure is trivial, $H = K = 0$, for cylinders $K = 0$, and for spheres $K = H^2$. In the second type of constraint, we only require that the block copolymer fills a wedge geometry that is space filling in the core. This more general wedge shape includes perfect spheres and cylinders as special cases, but it is also free to assume geometries that cannot be used to fill three-dimensional space to constant density. Thus the curvature characteristics obtained by minimizing the free energy under these less stringent constraints should be a better reflection of the *natural shape* of the microphase-separated block copolymers. Attempts to tile space with such general wedges may result in voids in the structure or self-intersection of the intermaterial dividing surface. A material for which the calculated curvature preferences lead to such a non-space-filling preferred wedge shape will form the space-filling structure (spheres, cylinders, cubic bicontinuous, or lamella) that is nearest in free energy to the preferred wedge. While all current theories of microphase-separated structures require specifying the structures first and then calculating and comparing free energies for these structures, we will show that the preference for a natural interfacial curvature, which depends on composition and molecular architecture, directs the choice of the actual space-filling structure formed. The difference between the free energy in the constrained perfect cylinders and in the less constrained preferred wedge shapes is used to understand the degree of long-range order in cylinder-forming materials.

In our energy calculations we ignore the fact that corona chains must fill the sharp edges of unit cells in cubic and hexagonal geometries. Thus we approximate the structures by isolated micelles. This same approximation was employed by Helfand and Wasserman in their early calculations for strongly segregated block copolymers.[28,30] The same unit cell approximation was utilized by Semenov[1] in the development of the self-consistent field approach, upon which our calculation is based. More recently, Olmsted and Milner[36] have developed techniques to approximate the energy associated with filling the sharp corners that result from packing domains on lattices. These calculations provide an upper bound on the energies of the structures, while calculations which neglect these sharp corners provide energetic lower bounds. Olmsted and Milner show that the ratio of the upper bound to lower bound energies are about 1.04 and 1.07 from hexagonally packed cylinders and bcc spheres, respectively. Thus the inaccuracy resulting from our neglect of the sharp corners of the unit cell is quite small. We must use this approximation in order to make calculations of general wedge shapes that are not constrained to conform to the geometries of known structures.

We start by calculating the free energy of a polymer brush, in the melt, grafted to a surface of arbitrary curvature. All energies in the following development are expressed in kT units. Using the Semenov approach, but ignoring the dead zone effect, the *action* is expressed as $J(\sigma) = NBh^2(\sigma)$. Here σ is the graft density, h is the brush height, N is the degree of polymerization, and $B = 3\pi^2/16N^2b^2$, where b is the Kuhn length. The free energy of stretching per chain is

$$g(\sigma) = \frac{1}{\sigma}\int_0^{\sigma} \mathrm{d}\sigma'\, J(\sigma) = \frac{1}{\sigma}\int_0^{h} \mathrm{d}h'\, \frac{\mathrm{d}\sigma'}{\mathrm{d}h'}\, J(h') \qquad (1)$$

The volume constraint for the "wedgelike" volume element with mean curvature H, Gaussian curvature K, and brush thickness h, is given by differential geometry:[19]

$$\frac{1}{3}Kh^3 + Hh^2 + h = Nv\sigma \qquad (2)$$

where v is the segmental volume. Therefore,

$$\frac{\mathrm{d}\sigma'}{\mathrm{d}h'} = \frac{1}{Nv}\{1 + 2Hh' + K(h')^2\} \qquad (3)$$

and

$$g(h) = \frac{\pi^2 h^2}{16Nb^2}\,\frac{1 + \frac{3}{2}Hh + \frac{3}{5}Kh^2}{1 + Hh + \frac{1}{3}Kh^2} \qquad (4)$$

This result for the stretching energy per chain is valid for melt brushes grafted to both convex ($H > 0$) and concave ($H < 0$) surfaces. It is exact for lamella, and for grafting on the concave side of cylindrical and spherical surfaces.

For a diblock copolymer layer, the free energy per chain consists of the stretching energies of blocks grafted onto opposite sides of the same interfacial surface as well as an interfacial energy contribution:

$$f = \frac{\pi^2 h_A^{\,2}}{16N_A b_A^{\,2}}\,\frac{1 - \frac{3}{2}Hh_A + \frac{3}{5}Kh_A^{\,2}}{1 - Hh_A + \frac{1}{3}Kh_A^{\,2}} + \frac{\pi^2 h_B^{\,2}}{16N_B b_B^{\,2}}\,\frac{1 + \frac{3}{2}Hh_B + \frac{3}{5}Kh_B^{\,2}}{1 + Hh_B + \frac{1}{3}Kh_B^{\,2}} + \gamma\frac{1}{\sigma} \qquad (5)$$

Here γ is the interfacial energy per unit area. The subscripts denote the A and B blocks of the copolymer. Note that the sign of H changes across the interface while the sign of K does not change.

In order to determine the preferred interfacial H and K, the free energy per chain, eq 5, is minimized subject to the two volume constraints:

$$\frac{1}{3}Kh_i^{\,3} - Hh_i^{\,2} + h_i = n_i V_i \sigma \qquad (6)$$

Here the subscript i refers to block A or B, $V_i = N_i v_i$ is the total volume of a block of component i, and n_i is the number of arms of component i, as in the I_2S architecture. Note that σ is the same for blocks on both sides of the interface. In this construct it is more convenient to use c_1 and c_2 as independent variables instead of H and K, which are expressed as $(c_1 + c_2)/2$ and c_1c_2, respectively, in eqs 5 and 6. In order to enforce the core-space-filling constraint in nonlamellar morphologies, we

further stipulate that one of the principal curvatures must be the reciprocal of the brush thickness on the concave side of the interface; the other principal curvature remains free to vary. We choose $c_1 = 1/h_A$ and $c_2 = \kappa c_1 = \kappa/h_A$. When $\kappa = 1$, the structure is spherical, when $\kappa = 0$, the structure is cylindrical, and when κ is negative, the interface has a negative Gaussian curvature or saddle shape, as found in bicontinuous structures.

Making these substitutions for H and K, incorporating the volume constraints, and introducing the variable r as the ratio of layer thicknesses, h_B/h_A allows the free energy to be written in the following form

$$f = \frac{\pi^2}{16}\left(\frac{n_A{}^3 V_A{}^2 \sigma^2}{N_A b_A{}^2} F_A + \frac{n_B{}^3 V_B{}^2 \sigma^2}{N_B b_B{}^2} F_B\right) + \gamma\frac{1}{\sigma} \qquad (7)$$

where F_A and F_B are

$$F_A = \frac{1 - \frac{3}{4}(1+\kappa) + \frac{3}{5}\kappa}{\left(1 - \frac{1}{2}(1+\kappa) + \frac{1}{3}\kappa\right)^3} \qquad (8)$$

$$F_B = \frac{1 + \frac{3}{4}(1+\kappa)r + \frac{3}{5}\kappa r^2}{\left(1 + \frac{1}{2}(1+\kappa)r + \frac{1}{3}\kappa r^2\right)^3} \qquad (9)$$

The volume constraints can be rearranged to give the following relationship for κ in terms of r and component volume fractions, ϕ_A and ϕ_B:

$$\kappa = \frac{\frac{1}{2}\phi_B - \phi_A r\left[1 + \frac{1}{2}r\right]}{\phi_A r\left[\frac{1}{2}r + \frac{1}{3}r^2\right] + \frac{1}{6}\phi_B} \qquad (10)$$

Minimization of the free energy with respect to the grafting density leads to the following relationship for the optimized σ:

$$\sigma = \left(\frac{\gamma/V}{\frac{\pi^2}{8}kT[n_A{}^2 l_A \phi_A F_A + n_B{}^2 l_B \phi_B F_B]}\right)^{1/3} \qquad (11)$$

With this value of σ substituted back into the free energy the following simplified form may be obtained:

$$\frac{f}{f_L} = \left(\frac{\epsilon^2 \phi_A F_A + \phi_B F_B}{\epsilon^2 \phi_A + \phi_B}\right)^{1/3} \qquad (12)$$

Here f/f_L is the ratio of the free energy per chain in a wedge of general curvature to the free energy of the same chain in a lamellar structure, and ϵ is the asymmetry parameter defined previously.

Figure 7 shows plots of f/f_L vs κ for symmetric diblock copolymers with $\epsilon = 1$ for A component volume fractions ranging from 0.05 to 0.45. For volume fractions of 0.3 or less, values of f/f_L less than 1.0 indicate a preference for structures with curved interfaces over flat lamellar interfaces. Since for constrained, perfect cylinders and spheres the free energy is only a function of one variable, σ, for which we have already minimized, the f/f_L values at $\kappa = 0$ and 1 correspond to the free energies of these constrained structures. The more general wedge shape corresponding to the preferred interfacial curvature is

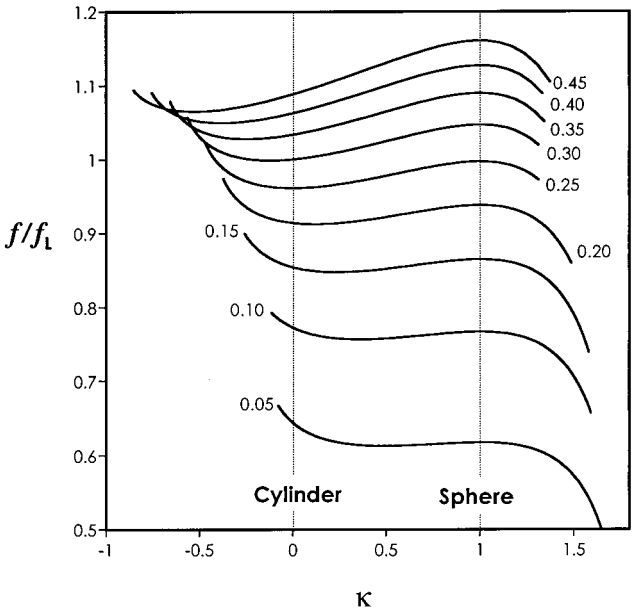

Figure 7. Ratio of the free energy of the preferred wedge geometry to the free energy of a lamellar structure at the same composition, f/f_L, as a function of κ for volume fractions of the minor component ranging from 0.05 to 0.45. These curves apply to a conformationally symmetric system with $\epsilon = 1$.

a function of the additional variable κ. With two free variables, the generalized Gaussian wedge represents a less constrained situation, and thus the free energy associated with this structure will be less than (or in special cases equal to) the free energies of the constrained geometries.

For each curve in Figure 7, as κ increases, f/f_L initially decreases, passes through a minimum, and then increases to a local maximum at $\kappa = 1$. Values of κ greater than 1 are unphysical since they indicate a higher curvature than a sphere, which is the highest possible interfacial curvature. The position of the minimum in the f/f_L curve indicates the preferred generalized wedge shape and thus the preferred interfacial curvature. This minimum occurs at a negative value of κ for volume fractions greater than 0.25, indicating a preference for saddle-shaped interfacial curvature which when strong enough, directs the formation of bicontinuous structures. At a volume fraction of 0.25 the minima occurs at $\kappa = 0$, indicating that the preferred interfacial curvature coincides exactly with constrained cylinders at this volume fraction, which is approximately in the middle of the range over which cylinders are observed experimentally. As the volume fraction decreases from 0.25 into the range in which spheres are experimentally observed, the minimum shifts to progressively higher values of κ. However, even at a volume fraction of 0.05, the minimum has only shifted up to $\kappa = 0.5$. In fact, the preferred value of κ can never even approach 1 (perfect spheres) because the local maximum remains at that position for every volume faction. However, this maximum becomes progressively lower as the volume fraction decreases so that in the range in which spheres are observed experimentally the value of f/f_L at this maximum is actually lower than the value corresponding to cylinders at $\kappa = 0$.

In order to determine the preferred interfacial curvature, we find the minima in f/f_L vs κ such as in Figure 7, which in general are also functions of the asymmetry, ϵ. Since the preferred Gaussian wedge shape corresponding to this preferred curvature cannot in general

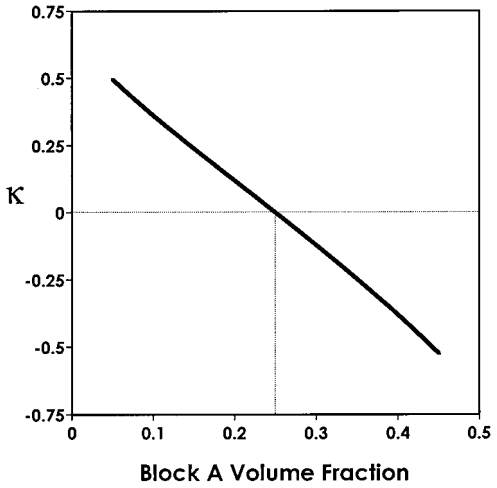

Figure 8. Calculated κ vs block A volume fraction for a conformationally symmetric AB diblock copolymer.

fill space, we must evaluate the energy penalties associated with deforming this preferred wedge into either constrained cylinders or constrained spheres. This energy penalty is the free energy of the constrained geometry minus the free energy of the preferred geometry. The constrained space-filling geometry actually formed by a real material corresponds to the lowest energy penalty for a given composition and molecular architecture.

Calculation Results and Discussion

Results were first calculated for a hypothetical linear diblock copolymer material with $N = 500$, $v_A = v_B = 140$ Å^3, $b_A = b_B = 6.7$ Å, and $\gamma = 0.014\ kT/$Å^2. These segmental volumes and Kuhn lengths represent averages of values for PS and PI, and the γ value is also appropriate for PS−PI systems. Thus this calculation is for a hypothetical series of linear diblocks with similar characteristics to PS−PI but with no conformational asymmetry. As shown in Figure 8, the κ corresponding to the preferred wedge shape is positive for small volume fractions of the minor component, passes through zero at a volume fraction of 0.25 and becomes negative for greater volume fractions. Figure 9 shows the resulting calculations of preferred HR_g and KR_g^2 vs the volume fraction of the A block and compares these curvature characteristics to those of perfect spheres and perfect cylinders. Curves are not plotted in the central portion of the figure, around 0.5 volume fraction, where the lamellar morphology is favored. The calculated HR_g curves for the preferred wedge shape and for the two constrained cases display the same general functional shape as the experimental plots in Figure 2, as well as similar actual values (when one adjusts for the difference between R_g and R_o). The mean curvature plots for preferred and constrained cases have a point of inversion symmetry at ($\phi_A = 0.5$, $HR_g = 0$).

The absolute value of the mean curvature of the constrained cylinder solution is always smaller than that of the constrained spherical solution. The preferred mean curvature intersects the constrained cylindrical mean curvature at volume fraction 0.25 (and 0.75), the same point at which κ and K are zero. Thus the preferred mean curvature coincides exactly with that of constrained cylinders at this single composition. As the volume fractions become highly asymmetric, approaching 0.0 or 1.0, the preferred mean curvature and that of the constrained spheres approach one another. KR_g^2 of the constrained spherical solution is always

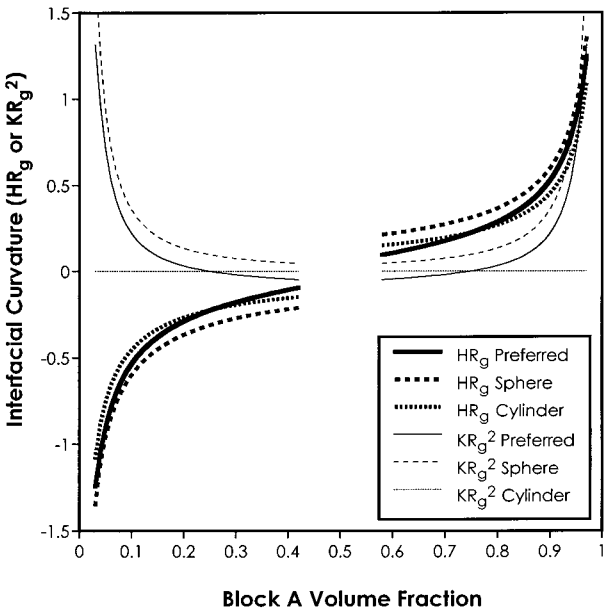

Figure 9. Calculated plots of preferred HR_g and KR_g^2 vs A block volume fraction for a conformationally symmetric AB diblock copolymer with $N = 500$. Also shown are plots representing cylindrically and spherically constrained HR_g and KR_g^2 values, as indicated by the legend.

positive, and it increases as the volume fractions become more asymmetric. The preferred Gaussian curvature is positive for volume fractions less than 0.25 (greater than 0.75), passes through zero, and is negative for more symmetric volume fractions. The Gaussian curvature of the constrained cylinders is always zero and thus intersects that of the preferred wedge shape at 0.25 volume fraction. The preferred Gaussian curvature passes through zero near the middle of the volume fraction range, 0.17−0.28, in which the cylindrical morphology is observed in approximately conformationally symmetric linear diblock copolymers. The preferred Gaussian curvature then becomes negative in the volume fraction range in which the cubic bicontinuous gyroid morphology is observed.

Figure 10 shows plots of f/f_L as a function of the volume fraction of component A for the preferred wedge shape as well as the constrained spherical and constrained cylindrical solutions. The functions are symmetric around 0.5 volume fraction, and thus the plots are only shown for volume fractions less than 0.5. The free energy of the less constrained preferred wedge shape is always less than the free energies of the constrained cylindrical and spherical solutions. The constrained cylindrical free energy coincides with the free energy of the preferred geometry at a volume fraction of 0.25 and is greater on either side of this point. The constrained spherical solution free energy becomes lower than that of the constrained cylinder solution for volume fractions less than 0.12, and the difference between the constrained spherical solution free energy and the preferred geometry free energy becomes smaller as the volume fractions become more asymmetric. Values of f/f_L less than 1.0 for any of these curves indicate stability relative to the lamellar structure. Of course we have not considered bicontinuous structures in our calculations. The purpose of the present calculations is not, however, to predict structural transitions, as this problem has been fully treated by others using the same type of theory.[1,25] The model may also be used to calculate block layer thicknesses, h_1 and h_2, and

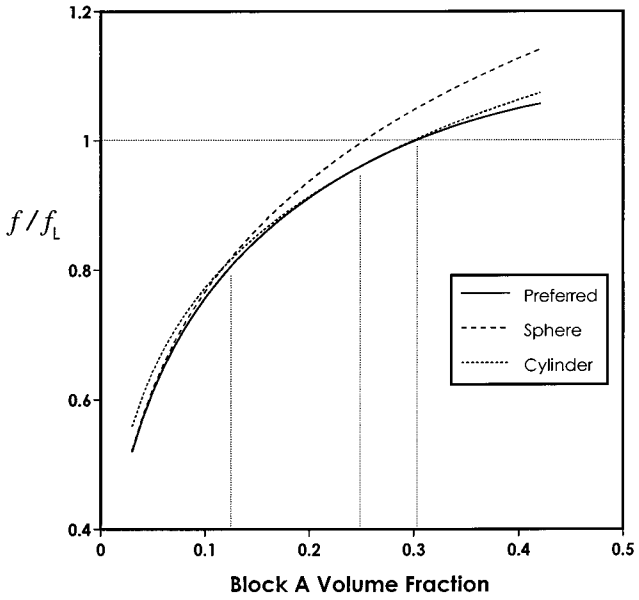

Figure 10. f/f_L as a function of A block volume fraction for a conformationally symmetric AB diblock copolymer. The free energy of the preferred geometry is compared to that of the cylindrically and spherically constrained geometries.

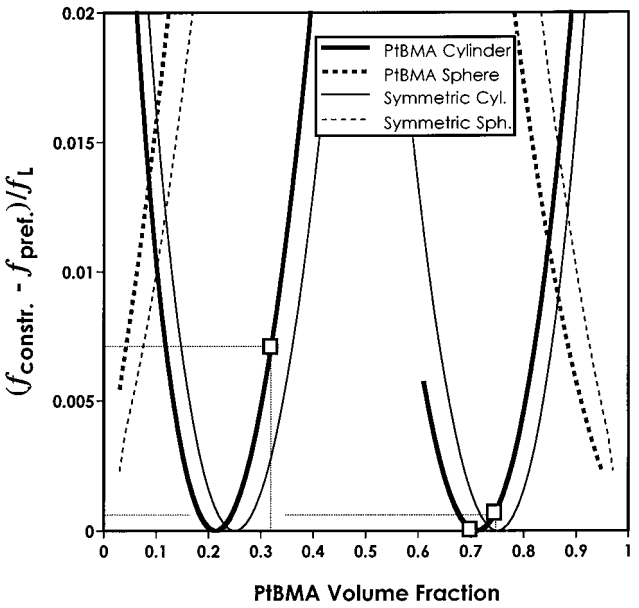

Figure 11. Free energy difference between a constrained geometry (sphere or cylinder) and the preferred geometry, in PI−PtBMA diblocks (PtBMA-32, -70, -75), as a function of PtBMA volume fraction. The energy differences are normalized by the lamellar free energy at the same composition. The three cylinder forming PI−PtBMA diblock samples are plotted as square symbols in the figure.

interfacial areas per molecule, A, as a function of volume fraction and chain architecture. These values are consistent with the experimental data tabulated in the Appendix for PS−PI and PS−PB linear diblocks as well as for the PI−PtBMA materials and the I_2S materials. Our purpose here, however, is to show that the observed structures form as a natural consequence of the interaction of the preferred interfacial curvature with the necessity of filling space uniformly, and that this interaction has implications for the degree of long-range order formed by the material.

The calculation of preferred interfacial curvature characteristics of linear conformationally asymmetric diblock copolymers can be carried out using the model outlined above with values of ϵ differing from unity. The preferred HR_g and KR_g^2 for PI−PtBMA block copolymers of the same approximate molecular weight as the samples in the experimental series are plotted in Figure 3 along with the experimental data points for HR_g. The constrained spherical and cylindrical solutions are also plotted in the figure for the PI−PtBMA system. Compared to Figure 9, the preferred interfacial curvature characteristics are slightly asymmetric with respect to the 0.5 volume fraction of PtBMA, reflecting the modest but notable conformational asymmetry in this diblock. The interfacial curvatures are higher when the PtBMA block with its longer Kuhn length (easier to stretch) is on the concave side of the interface than they are when the PI block with its shorter Kuhn length (harder to stretch) is on the concave side of the interface. Over the range of PtBMA volume fractions there is reasonable agreement in the trends displayed by the experimental and calculated HR_g values.

In Figure 3 the preferred mean and Gaussian curvatures coincide with the constrained cylindrical solution values at volume fractions of 0.22 and 0.72. The two samples at 0.70 and 0.75 volume fraction, which display a high degree of long-range order, are close to one of these coincidence points, indicating that these materials naturally prefer a cylindrically curved geometry. The sample at 0.32 volume fraction, which displayed poor long-range order, does not fall so near to the other coincidence point. Even though the cylindrical solution is the best space filling structure for this material, it actually must experience a significant degree of frustration in order to fill space in this geometry. Figure 11 shows a plot of the difference in free energy between the constrained cylindrical solution and the preferred solution (normalized by the free energy of the lamellar structure at the same composition) as a function of volume fraction for the PI−PtBMA diblocks. Included for reference on the same graph is the same free energy difference for a symmetric, $\epsilon = 1$, diblock. This plot clearly indicates that the well-ordered cylinders at 0.70 and 0.75 volume fraction experience significantly less packing frustration in filling space than the poorly ordered cylinders at 0.32 volume fraction.

The calculation of preferred interfacial curvature characteristics of architecturally asymmetric I_2S block copolymers can be carried out using the model outlined above with values of ϵ of 1.78 (two PI arms in the corona) and 0.56 (two PI arms in the core). The preferred HR_g and KR_g^2 for I_2S block copolymers of the same approximate molecular weight as the samples in the experimental series are plotted in Figure 4 along with the experimental data points for HR_g. The constrained spherical and cylindrical solutions are also plotted in the figure for the I_2S system. Compared to Figure 9, the preferred interfacial curvature characteristics are markedly asymmetric with respect to 0.5 volume fraction of the single PS graft, reflecting the architectural asymmetry in this graft copolymer. The interfacial curvatures are higher when the two PI blocks per molecule are in the corona and the single PS block is in the core than when the situation is reversed. This is due to the lateral crowding and resulting additional chain stretching of the two PI blocks on one side of the interface. A numerical solution for the preferred curvature cannot be obtained for volume fractions less than 0.23, and thus the calculated curves end at this point. Over the range of PS volume fractions there is reasonable agreement in the trends displayed by the experimental and calculated HR_g values.

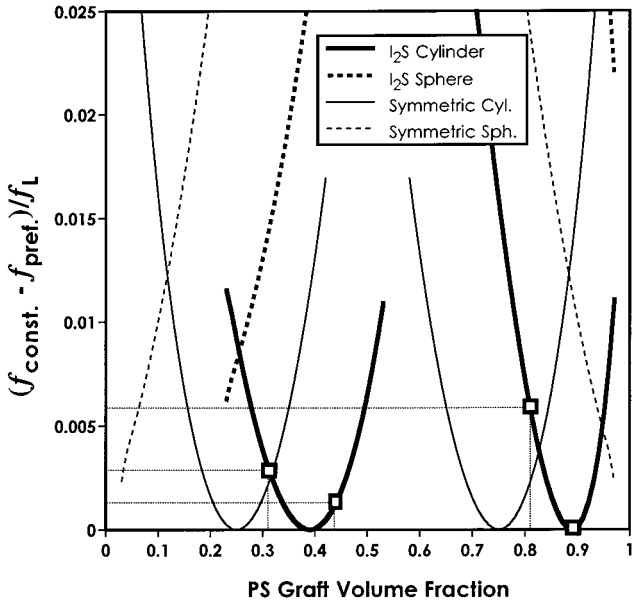

Figure 12. Free energy difference between a constrained geometry (sphere or cylinder) and the preferred geometry, in I_2S simple graft copolymers (I_2S-1, -2, -4, -5), as a function of PS graft volume fraction. The energy differences are normalized by the lamellar free energy at the same composition. The four cylinder forming I_2S samples are plotted as square symbols in the figure.

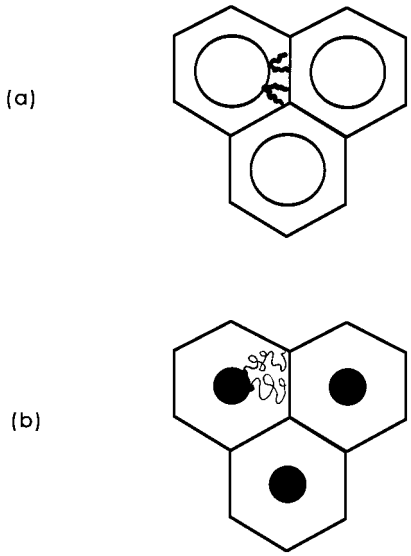

Figure 13. Comparison of cylindrical domains in the I_2S materials with (a) two short highly stretched corona chains per molecule (I_2S-4 and -5) and (b) a single longer and less highly stretched corona chain per molecule (I_2S-1 and -2).

In Figure 4 the preferred mean and Gaussian curvatures coincide with the mean and Gaussian curvatures of the constrained cylindrical solution at volume fractions of 0.39 and 0.89. Samples I_2S-4 and -5, with PS volume fractions of 0.31 and 0.44, which display a high degree of long-range order, are close to one of these coincidence points, indicating that these materials naturally prefer a cylindrically curved geometry. The architectural asymmetry has shifted the values of preferred and constrained interfacial curvatures (both mean and Gaussian) such that the difference between the preferred curvature and constrained cylindrical curvature is small over a relatively broad range of volume fractions on the left hand side of the diagram. In Figure 12 this is reflected in low values of the free energy difference between constrained cylinders and the preferred geometry for these two samples. On the other side of the diagram, I_2S-2, with a PI volume fraction of 0.81, is experimentally observed to have a morphology of randomly oriented cylinders with convoluted trajectories (wormlike micelles). This sample, which displays no long-range order at all, occurs where there is a rather large difference between the preferred curvature characteristics and the curvature characteristics of space-filling cylinders. Thus this sample will experience a large amount of frustration, quantified by the free energy difference for this sample in Figure 12, in assuming a cylindrical morphology. The degree of such geometric frustration appears to be strongly correlated with poor or, in this case, nonexistent, long-range order. Sample I_2S-1, at 0.89 PS volume fraction, occurs right at the intersection of the preferred curvature with the constrained cylindrical curvature characteristics, and thus this sample is expected to readily form well ordered cylinders. In Figure 12 this sample falls almost exactly at the minimum free energy difference between constrained cylinders and the preferred geometry.

In fact, I_2S-1 was observed to form a poorly ordered morphology of hexagonally packed cylinders. This appears to contradict our proposed correlation between the degree of long-range order and the deviation from the preferred curvature free energy. However, while we believe that the preferred curvature characteristics play a major role, long wavelength (phonon-like) fluctuations and defects are expected to also influence long-range order. The phenomenological description of long wavelength fluctuations and defects for the hexagonal cylinder phase of block copolymers is identical to that for the columnar phase in liquid crystals. Such a description involves a set of elastic constants associated with the various modes of deformation[35] and the free energy cost for various defects. Calculation of these properties is beyond the scope of the present work and will be pursued in the future. However, as illustrated in Figure 13, it is intuitive that thinner cylinders in a softer matrix will lead to smaller elastic constants and hence larger fluctuations from the perfect lattice structure. Due to the I_2S architecture, the shift in the volume fraction range in which cylinders are observed leads to smaller corona volume fractions for I_2S-4 and -5 than in diblock cylinders. Due to the additional crowding of the two PI chains per molecule, the corona chains are more highly stretched than in diblock cylinders. Thus in samples I_2S-4 and -5 the cylinders reside in the matrix of short, rather highly stretched corona chains. These structures are therefore expected to have large elastic constants and are hard to deform. In the I_2S-1 and 2-samples, again because of the shift in volume fractions for the cylindrical morphology, the PS corona blocks occupy a larger volume fraction than in linear diblocks. These long PS corona chains are less stretched than in diblock cylinders and provide a much softer matrix. Therefore, we expect larger lattice deformation due to thermal fluctuations.

Only on the basis of the consideration of long wavelength deformations, we would conclude that if sample I_2S-2 shows no long-range order, then certainly sample I_2S-1—with thinner cylinders in a matrix of longer PS corona chains—should show even less tendency toward long-range order. The fact that long-range order reappears in I_2S-1 indicates the importance of the preferred interfacial curvature arguments that have been the main point of this paper.

Table 3. Experimental Data from the Literature on Diblock Copolymers

A block	B block	A M_n	B M_n	lattice param (Å)	domain dimension (Å)	N	R_o (Å)	A vol fraction	HR_o	ref
					Spheres					
PS	PB	10 500	113 000	563	116	2190	291	0.07	−2.51	27
PS	PB	56 600	10 900	433	90	745	182	0.82	2.02	27
PS	PB	7 200	33 000	323	86	679	163	0.16	−1.90	28
PS	PB	8 000	40 000	358	107	816	179	0.15	−1.67	28
PS	PB	11 000	47 000	427	108	975	196	0.17	1.81	28
PS	PB	12 000	163 000	624	109	3129	348	0.06	−3.19	28
PS	PB	13 000	59 000	485	128	1216	218	0.16	−1.71	28
PS	PB	15 000	32 000	450	112	736	171	0.28	−1.53	28
PS	PB	15 000	83 000	566	122	1678	256	0.13	−2.10	28
PS	PI	15 000	75 000	531	130	1245	221	0.15	−1.70	28
PS	PI	51 000	227 000	1,166	100	3822	388	0.17	−3.88	28
PS	PI	47 000	17 000	531	163	701	175	0.71	1.07	28
PS	PI	62 000	12 000	473	68	771	185	0.82	2.73	28
PS	PI	125 000	20 000	704	85	1494	259	0.85	3.05	28
PS	PI	176 000	20 000	762	96	1983	300	0.89	3.12	28
PS	PI	185 000	34 000	970	130	2275	319	0.83	2.45	28
PS	PI	251 000	71 000	1443	170	3452	390	0.76	2.29	28
PS	PI	513 000	144 000	231	320	7040	557	0.76	1.74	28
PS	PI	158 000	27 000	843	150	1913	293	0.84	1.95	28
PS	PI	116 000	28 000	808	125	1525	260	0.78	2.08	28
PS	PI	67 000	13 000	279	66	834	193	0.82	2.92	29
PS	PI	125 000	20 000	350	80	1494	259	0.85	3.24	29
PS	PI	176 000	26 000	408	94	2072	305	0.86	3.25	29
PS	PI	185 000	34 000	463	127	2275	319	0.83	2.51	29
PS	PI	251 000	71 000	739	171	3452	390	0.76	2.28	29
PS	PI	513 000	144 000	1224	319	7040	557	0.76	1.74	29
PS	PI	13 120	68 880	404	106	1137	211	0.14	−1.99	31
					Cylinders					
PS	PB	12 000	22 000	288	78.5	522	145	0.32	−0.92	30
PS	PB	15 000	35 000	336	100	791	178	0.27	−0.89	30
PS	PB	20 000	50 000	370	103	1116	211	0.25	−1.02	30
PS	PB	25 000	72 000	440	126	1571	250	0.23	−0.99	30
PS	PB	36 000	121 000	565	158	2583	319	0.20	−1.01	30
PS	PB	49 000	76 000	635	196.5	1875	275	0.35	−0.70	30
PS	PB	49 000	124 000	743	196.5	2763	331	0.25	−0.84	30
PS	PB	52 000	24 000	328	97.5	943	200	0.65	1.03	30
PS	PB	56 000	26 000	336	99	1018	208	0.65	1.05	30
PS	PB	49 000	12 400	360	91	700	175	0.77	0.96	30
PS	PB	49 000	21 500	447	137.5	868	193	0.66	0.70	30
PS	PB	52 500	22 500	442	110	920	198	0.66	0.90	30
PS	PB	306 000	115 000	550	165	5064	467	0.69	1.41	30
PS	PI	12 500	35 600	360	93.5	643	160	0.24	−0.86	30
PS	PI	229 000	309 000		330	6735	525	0.39	−0.80	30
PS	PI	12 600	6 000	175	52	209	95	0.65	0.91	30
PS	PI	29 000	7 000	272	64	381	130	0.78	1.01	30
PS	PI	93 500	27 500		92.5	1301	239	0.75	1.29	30
PS	PI	116 000	28 000		115	1525	260	0.78	1.13	30
PS	PI	173 000	48 000		115	2366	323	0.76	1.40	30
PS	PI	237 000	66 000		145	3244	378	0.76	1.30	30
PMMA	PI	21 000	46 000	436	138	885	187	0.27	−0.68	30
PS	PI	13 120	68 880	365	71.6	1137	211	0.14	−1.48	31
PS	PI	13 120	68 880	378	74.7	1137	211	0.14	−1.41	31
					Lamella					
PS	PI	70 000	70 000	590		1700	266	0.47	0	14
PS	PI	23 000	8 000	220		338	121	0.72	0	14
PS	PI	23 000	17 500	290		478	142	0.54	0	14
PS	PI	23 000	21 000	310		529	149	0.49	0	14
PS	PI	23 000	28 000	360		632	161	0.42	0	14
PS	PI	30 000	17 500	340		545	152	0.60	0	14
PS	PI	46 900	17 000	450		700	175	0.71	0	14
PS	PI	29 000	34 000	500		778	179	0.43	0	14
PS	PI	62 000	43 000	660		1227	228	0.56	0	14
PS	PB	32 000	48 000	445		1195	220	0.36	0	14
PS	PB	35 500	54 500	490		1348	233	0.36	0	14
PS	PB	71 000	46 000	740		1532	253	0.57	0	14
PS	PB	48 900	32 400	460		1068	212	0.56	0	14
PS	PI	11 130	9 870	172		252	103	0.50	0	32
PS	PI	12 400	18 600	243		392	126	0.37	0	32
PS	PI	22 050	26 950	319		607	158	0.42	0	32
PS	PI	25 300	29 700	340		679	167	0.43	0	32
PS	PI	49 470	47 530	463		1173	221	0.48	0	32
PS	PI	62 220	39 780	503		1181	224	0.58	0	32
PS	PI	34,696	40,404	420		926	195	0.43	0	33
PS	PI	61,950	43,050	670		1227	228	0.56	0	15
PS	PI	26,600	22,100	387		580	156	0.51	0	34

Conclusions

In this study we have shown that the minimization of a single chain free energy in the strong segregation limit can yield information about the effect of molecular architecture, conformational asymmetry, and composition on preferred interfacial curvature. The calculation of preferred H and K does not take into account the packing constraints necessary to fill space when domains are packed on a lattice. Nor does it account for the packing problems inherent in filling the centers of tripod or tetrapod connectors necessary in cubic bicontinuous structures. These packing constraints can result in deviations from constant interfacial mean curvature. These deviations, often too small to detect experimentally, do not pose a problem for the current approach even when they are significant. The preferred H and K represent the preferences of the molecules, neglecting the fact that they must pack onto a lattice. The structure actually chosen by the material is that structure which minimizes the distortion away from the preferred curvature when material fills space on a lattice.

The preferred mean curvature is negative when the reference phase is the minor component and is on the concave side of the interface and is positive when the reference phase is the major component on the convex side of the interface (in the matrix). The absolute value of the preferred mean curvature becomes larger as the volume fractions become asymmetric. The calculated values of preferred mean curvature were found to agree reasonably well with experimentally measured interfacial curvatures in PS−PI and PS−PB diblock copolymers as well as in conformationally asymmetric PI−PtBMA diblocks and architecturally asymmetric simple graft I_2S block copolymers. In these systems there are asymmetric shifts in the interfacial curvature vs volume fraction behavior, quite strong in the case of I_2S materials, due to conformational and architectural asymmetry.

In both the PI−PtBMA and I_2S materials a large disparity in the ability of cylindrical morphologies to form long-range order was observed between cylindrical phases on opposite sides of the morphology diagram. PI−PtBMA cylinders with PI in the matrix phase formed poor long-range order, while cylinders with PtBMA in the matrix phase formed tremendous long-range order. I_2S cylinders with two PI blocks per molecule in the matrix phase formed excellent long-range order, while cylinders with the single PS block per molecule in the matrix formed poor or even nonexistent long-range order. The general trends in long-range order of cylindrical structures can be correlated to the difference in free energy between a constrained cylindrical geometry and the preferred geometry. When the preferred geometry, which is in general not space filling, must be significantly distorted to form the space-filling cylindrical geometry, the system experiences frustration which manifests, itself in poorer long-range order.

Acknowledgments. We wish to acknowledge Darrin J. Pochan for providing TEM and SAXS data for this paper and Chin Lee for useful discussions. S.P.G. acknowledges funding from the Army Research Office in the form of an Army Young Investigator Award DAAH04-95-I-0305. Use of TEM instrumentation in the W. M. Keck Electron Microscopy Laboratory at the University of Massachusetts−Amherst is acknowledged, as is the use of central facilities of the Materials Research Science and Engineering Center (MRSEC) at the University of Massachusetts. Z.-G.W acknowledges support from the National Science Foundation (Grant Nos. ASC-9217368 and DMR-9531914), the Camille and Henry Dreyfus Foundation (Award No. TC-96-063) and the Alfred P. Sloan Foundation (Award No. BR-3508).

References and Notes

(1) Semenov, A. N. *Sov. Phys. JETP* **1985**, *61*, 733.
(2) Pochan, D. J.; Gido, S. P.; Pispas, S.; Mays, J. W.; Ryan, A. J.; Fairclough, J. P. A.; Hamley, I. W.; Terrill, N. J. *Macromolecules* **1996**, *29*, 5091.
(3) Hadziioannou, G.; Mathis, A.; Skoulios, A. *Colloid Polym. Sci.* **1979**, *257*, 22.
(4) Albalak, R. J.; Thomas, E. L. *J. Polym. Sci., Polym. Phys. Ed.* **1993**, *31*, 37.
(5) Pochan, D. J.; Gido, S. P.; Pispas, S.; Mays, J. W. *Macromolecules* **1996**, *29*, 5099.
(6) Tselikas, Y.; Iatrou, H.; Hadjichristidis, N.; Liang, K. S.; Mohanty, K.; Lohse, D. J. *J. Chem. Phys.* **1996**, *105*, 2456.
(7) Pochan, D. J.; Gido, S. P.; Zhou, J.; Mays, J. W.; Whitmore, M.; Ryan, A. J. *J. Polym. Sci., Polym. Phys. Ed.*, in press.
(8) Israelachvili, J. N. *Intermolecular and Surface Forces*; Academic Press: New York, 1985.
(9) Hyde, S. T. *Coll. Phys.* **1990**, *C7*, 209.
(10) Anderson, D. M.; Thomas, E. L. *Macromolecules* **1988**, *21*, 3221.
(11) Gido, S. P.; Thomas, E. L. *Macromolecules* **1994**, *27*, 849.
(12) Gido, S. P.; Gunther, J.; Thomas, E. L.; Hoffman, D. *Macromolecules* **1993**, *26*, 4506.
(13) Thomas, E. L.; Anderson, D. M.; Henkee, C. S.; Hoffman, D. *Nature* **1988**, *334*, 598.
(14) Helfand, E.; Wasserman, Z. R. *Macromolecules* **1976**, *9*, 879.
(15) Hashimoto, T.; Todo, A.; Itoi, H.; Kawai, H. *Macromolecules* **1977**, *10*, 377.
(16) Reference deleted in revision.
(17) Reference deleted in revision.
(18) Reference deleted in revision.
(19) Safran, S. A. *Statistical Thermodynamics of Surfaces, Interfaces, and Membranes*; Addison-Wesley: Reading, MA, 1994; Vol. 90.
(20) Schwarz, H. A. *Gesammelte Mathematische Abhandlungen*; Springer: Berlin, 1890.
(21) Hoffman, D. A. *Coll. Phys.* **1990**, *51*, C7−197.
(22) Gido, S. P.; Schwark, D. W.; Thomas, E. L.; Goncalves, M. *Macromolecules* **1993**, *26*, 2636.
(23) Matsen, M. M.; Bates, F. S. *Macromolecules* **1996**, *29*, 7641.
(24) Olvera de la Cruz, M.; Sanchez, I. C. *Macromolecules* **1986**, *19*, 2501.
(25) Milner, S. T. *Macromolecules* **1994**, *27*, 2333.
(26) Yamakawa, H. *Modern Theory of Polymer Solutions*; Harper & Row: New York, 1971.
(27) Thomas, E. L.; Kinning, D. J.; Alward, D. B.; Henkee, C. S. *Macromolecules* **1987**, *20*, 2934.
(28) Helfand, E.; Wasserman, Z. R. *Macromolecules* **1978**, *11*, 960.
(29) Hashimoto, T.; Fujimura, M.; Kawai, H. *Macromolecules* **1980**, *13*, 1660.
(30) Helfand, E.; Wasserman, Z. R. *Macromolecules* **1980**, *13*, 994.
(31) Sakurai, S.; Kawada, H.; Hashimoto, T.; Fetters, L. J. *Macromolecules* **1993**, *26*, 5796.
(32) Hashimoto, T.; Shibayama, M.; Kawai, H. *Macromolecules* **1980**, *13*, 1237.
(33) Hasegawa, H.; Hashimoto, T.; Kawai, H.; Lodge, T. P.; Amis, E. J.; Glinka, C. J.; Han, C. C. *Macromolecules* **1985**, *18*, 67.
(34) Winey, K. I. Ph.D. Thesis, University of Massachusetts, 1991.
(35) de Gennes, P.-G.; Prost, J. *The Physics of Liquid Crystals*, 2nd ed.;Clarendon Press, Oxford, U.K., 1993.
(36) Olmsted, P. D.; Milner, S. T. *Phys. Rev. Lett.* **1994**, *72*, 936.

MA9703564